Using spectrally-selective radiofrequency pulses to enhance lactate signal for diffusion-weighted MRS measurements in vivo

Eloïse Mougel, Sophie Malaquin, Mélissa Vincent, Julien Valette

Journal of Magnetic Resonance 334 (2022) 107113

Contents lists available at ScienceDirect

Journal of Magnetic Resonance

journal homepage: www.elsevier.com/locate/jmr

Using spectrally-selective radiofrequency pulses to enhance lactate signal for diffusion-weighted MRS measurements in vivo

Eloïse Mougel, Sophie Malaquin, Mélissa Vincent, Julien Valette *

Université Paris-Saclay, CEA, CNRS, MIRCen, Laboratoire des Maladies Neurodégénératives (UMR 9199), Fontenay-aux-Roses, France

ARTICLE INFO

Article history:
Received 30 June 2021
Revised 2 November 2021
Accepted 23 November 2021
Available online 26 November 2021

Keywords:
DW-MRS
J-coupling
Frequency selective pulse
Polychromatic pulse
Lactate

ABSTRACT

Measurement of lactate diffusion properties using diffusion-weighted magnetic resonance spectroscopy in vivo may allow elucidating brain lactate cellular compartmentation, which would be of great importance for neuroscience. However, measuring lactate signal is complicated by low signal-to-noise ratio due to low lactate concentration and J-modulation of its 1.3 ppm peak.

In this work, we assess the benefits of using a diffusion-weighting spin echo block and spectrally selective refocusing pulses to suppress the effect of J-coupling on the 1.3 ppm lactate resonance, by not refocusing its coupling partner at 4.1 ppm. Two different kinds of spectrally selective pulses, either polychromatic or single-band, are evaluated in the mouse brain at 11.7 T. Almost complete suppression of J-modulation is shown, resulting in an approximately two-fold signal increase as compared to a reference STE-LASER sequence (for the specific diffusion times used in this work). Repeated measurements confirm that lactate diffusion-weighted signal attenuation is measured with an approximately two-fold precision.

1. Introduction

The idea has been proposed that measuring brain lactate (Lac) diffusion properties, using diffusion-weighted MR spectroscopy (DW-MRS), may shed some light about lactate distribution between extracellular and intracellular space, due to different diffusion properties within these two compartments [1]. More recently, it has been suggested that morphological differences between astrocytes and neurons are large enough to induce different intracellular diffusion properties, as assessed by measuring the diffusion of cell-specific metabolites such as astrocytic myo-inositol (Ins) and neuronal N-acetyl aspartate (NAA) [2–4], so that DW-MRS might even allow distinguishing astrocytic lactate from neuronal lactate [5]. This opens fantastic perspectives to non-invasively study the cellular compartmentation of brain lactate, which is tightly linked to the controversial astrocyte-to-neuron lactate shuttle hypothesis [6], whereby the existence of a lactate concentration gradient, as recently confirmed using FRET imaging [7], allows lactate produced in excess in astrocytes to be released in the extracellular space and taken up by neurons to sustain (at least partially) neuronal energy needs.

Measuring brain lactate diffusion properties with DW-MRS is however critically limited by the low signal-to-noise ratio (SNR), due to low lactate concentration (0.5–1 mM) and, on top of that, to the fact that its prominent CH_3 peak at 1.3 ppm is J-coupled with the CH group (resonating at 4.1 ppm and barely detectable on spectra). Hence, DW-MRS sequence must be carefully chosen to maximize lactate signal. Methods have been proposed to optimize detection of the 1.3-ppm lactate peak and separate it from macromolecules at 1.2–1.4 ppm, based on comparison/difference of spectra acquired at different echo times (TE) [8], or on MEscher-GArwood (MEGA) J-editing [9]. However these methods require very long TE (>144 ms), which becomes impractical at high field because of shorter T2 relaxation times [10]. Moreover, these methods require at least two acquisitions which are then subtracted, which may lead to artifacts. Finally, incorporating diffusion gradients in such sequences is not trivial if one wants to avoid cross-terms with other gradients.

In most of our recent works, including in Ligneul *et al.* [5] where lactate signal at high *b*-values was interpreted as reflecting lactate compartmentalized primarily within astrocytes in control mice, but primarily within neurons in a mouse model of astrocyte reactivity, we used the STE-LASER sequence [11]. This sequence consists of a non-localized diffusion-weighted stimulated echo (STE) block, followed by a LASER localization block. The advantage of STE-based diffusion-weighting is that it allows high b-values

* Corresponding author.
E-mail address: julien.valette@cea.fr (J. Valette).

https://doi.org/10.1016/j.jmr.2021.107113
1090-7807/

(or long diffusion time t_d) to be reached, while keeping TE relatively short and, thus, mitigating J-modulation (and T_2 relaxation). Hence, while STE results in the loss of half the magnetization as compared to a spin echo (SE), in general there is no benefit to perform SE-based diffusion-weighting, at least for J-coupled metabolites such as lactate.

In a weakly coupled spin system evolving during a spin echo, J-coupling effect on any resonance can be canceled by refocusing only that particular resonance. In the context of lactate diffusion measurement with STE-LASER, replacing the STE diffusion block by a SE diffusion block, where the refocusing pulses selectively refocuses the 1.3 ppm, but not the 4.1 ppm resonance, will cancel the effect of J-coupling. The goal of this work was to assess to what extent such an approach allows better characterization of lactate signal attenuation, for diffusion times of ~50 ms (i.e. similar to the one which allowed observing very significant alteration of lactate signal attenuation in a mouse model of astrocyte reactivity [5]). Besides the constraint on refocusing the lactate resonance at 1.3 ppm, but not at 4.1 ppm, we imposed the two following specifications:

- In the long-term perspective of comparing lactate diffusion to cell-specific intracellular metabolites to elucidate lactate compartmentation, the pulse must also refocus the NAA at 2 ppm and the Ins at 3.5 ppm, so that these peaks are visible on spectra.
- Since macromolecules (MM) at 1.4 ppm largely overlap with lactate, it is necessary to properly quantify MM signal. Hence we propose to refocus the isolated 0.9-ppm MM peak, in order to provide a reliable estimate of overall MM contribution.

Two different kinds of spectrally-selective refocusing pulses were evaluated: either a polychromatic (PC) pulse with several bands refocusing only the resonances of interest (as previously used by Shemesh et al. [4,12]), or a single-band (SB) pulse refocusing the whole ~ 0.1–4.0 ppm range.

2. Methods

Two series of independent experiments were conducted to evaluate the precision on lactate signal attenuation measurement: first, diffusion measurements using standard STE-LASER sequence (Fig. 1A), used as a reference, were compared to a "PC-SE-LASER" sequence, i.e. a sequence where the diffusion-weighted STE block is replaced by a diffusion-weighted SE block where refocusing is achieved with a polychromatic pulse (Fig. 1B and 1C); second, diffusion measurements using standard STE-LASER sequence were compared to SB-SE-LASER, i.e. a SE-LASER sequence where refocusing is now achieved with a single-band (0.1–4.0 ppm range) refocusing pulse (Fig. 1B and 1D).

2.1. Sequences design

The STE-LASER used as reference is as described in the original article [11], where the STE block consists in three broad pulses and diffusion gradients, and the LASER block contains six adiabatic full passage (HS1) slice-selective pulses (Fig. 1A).

For the SE block in SE-LASER sequences (Fig. 1B), excitation is achieved by an adiabatic half passage pulse, and refocusing is performed by a selective pulse consisting either in the polychromatic (Fig. 1C) or the single-band pulse (Fig. 1D). Diffusion gradients are positioned symmetrically around the refocusing pulse. The LASER block is the same as in the STE-LASER, with a 25-ms duration in all cases.

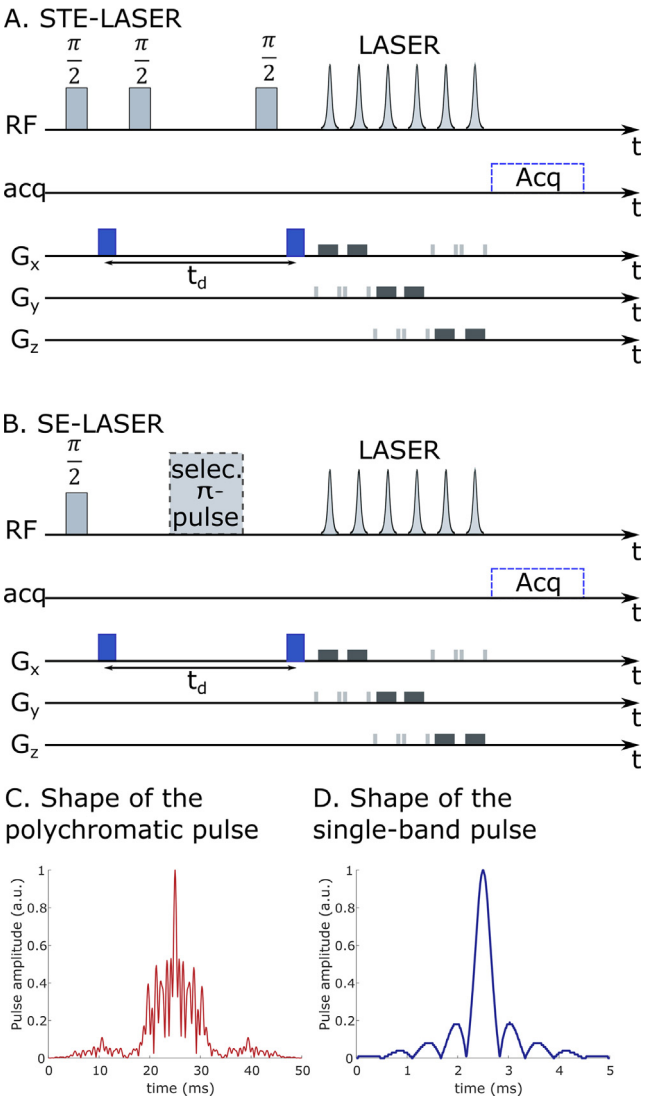

Fig. 1. Chronograms of A) STE-LASER used as reference, and B) SE-LASER where selective refocusing is performed in the SE block. Two selective radiofrequency (RF) pulses were generated with the Shinnar-Leroux algorithm: C) polychromatic RF pulse that is selective on four bands of interest, and D) selective single-band RF pulse on the 0.1–4.0 ppm range. Diffusion gradients are indicated in blue. The slice selection gradients and the spoiler gradients are in dark gray and light gray, respectively. (For interpretation of the references to colour in this figure legend, the reader is referred to the web version of this article.)

2.2. Generation of RF pulses

The polychromatic pulse was generated by summing four elementary pulses (complex summation) modulated at four different frequency offsets: 3.5 ppm (Ins), 2 ppm (NAA), 1.3 ppm (Lac) and 0.9 ppm (MM). The elementary pulse was generated using the Shinnar-Leroux (SLR) algorithm [13], with Pauly's tool implemented in Matlab (The MathWorks, Natick, Massachusetts, USA). Time × bandwidth product was set to 3.9 and pulse duration was then set to 50 ms, resulting in an elementary pulse bandwidth of 78 Hz. Target in-phase ripple amplitude was 0.1% and target out-phase ripple amplitude was 0.01%.

The single-band pulse refocusing the 0.1–4.0 ppm band was also generated with the SLR algorithm. Time-bandwidth product was set to 8.3, and ripple amplitudes were set to 0.1% and 0.45% for in-phase and out-phase, respectively. Pulse duration was set to 5 ms, resulting in 1660-Hz bandwidth. A 1300-Hz offset was applied to center the pulse at the middle of the 0.1–4.0 ppm band.

2.3. Evaluating pulse performance with numerical simulations

Pulse performance was evaluated with a homemade Bloch simulator implemented in Matlab. Simulations were performed for isochromats from −1.3 to 6.7 ppm, and for B_1 intensities from 0.05 to 10.15 μT for the PC case, and from 0.05 to 60.55 μT for the SB case. To facilitate visualization of results, simulations were performed for an inversion, i.e. for magnetization originally along B_0 (+z).

Then, metabolite spectra were simulated for both SE-LASER sequences, using home-made Matlab routines to compute the evolution of the density matrix, with chemical shifts and J-coupling constants as reported in [14]. This allows the efficiency of J-coupling suppression on lactate to be evaluated, and to simulate the basis-set for quantification of in vivo spectra (see below).

2.4. In vivo experiment

All experimental protocols were reviewed and approved by the local ethics committee (CETEA N°44), and authorized by the French Ministry of Education and Research. They were performed in an approved facility (authorization #B92-032–02), in strict accordance with recommendations of the European Union (2010–63/EEC). All efforts were made to minimize animal suffering, and animal care was supervised by veterinarians and animal technicians. Mice were housed under standard environmental conditions (12-hour light–dark cycle, temperature: 22 ± 1 °C and humidity: 50%) with ad libitum access to food and water.

Experiments were performed on an 11.7 T BioSpec Bruker scanner interfaced to PV6.0.1 (Bruker, Ettlingen, Germany). A quadrature surface cryoprobe (Bruker, Ettlingen, Germany) was used for transmission and reception. Two 3-month-old C56-BL7 mice were anesthetized with ∼1.5% isoflurane and maintained on a stereotaxic bed with a bite and two ear bars. Throughout the experiments, body temperature was monitored and maintained at ∼ 36 °C by warm water circulation. Breathing frequency was monitored using PC – SAM software (Small Animal Instruments, Inc., Stony Brook, NY).

A 31.5 μL (7 × 1.5 × 3 mm^3) spectroscopic voxel was placed around the hippocampus, and shimming was performed using Bruker's Mapshim routine, yielding a water linewidth of ∼ 16 Hz. 8 series of 32 repetitions were acquired for two different *b*-values (*b* = 0.02 ms/μm², which is the minimal *b*-value allowing efficient spoiling of unwanted coherences, and 8 ms/μm²) with the PC-SE-LASER in the first experiment (Fig. 2A) and SB-SE-LASER in the second experiment (Fig. 2B), and in both experiments with the STE-LASER as reference. Each series of acquisitions was interleaved according to the pattern in Fig. 2C, to mitigate potential biases arising over the course of the experiment (such as degraded shim or variations of lactate concentration). For STE-LASER acquisitions, water suppression was achieved using a VAPOR module plus an additional water suppression pulse inserted in the mixing time

A.

Sequences	Pulses	Diffusion Time(t_d) / Echo Time (TE)/ Repetition Time (TR)	Acquisition LASER parameters	Other sequence parameters
DW-non-selective stimulated echo sequence (STE-LASER)	$\frac{\pi}{2}$: Broad pulse: 0.1 ms.	t_d = 53.2 ms TE = 8.4 ms TR = 2 s (4 s for MM)	TE = 25 ms Adiabatic pulses: HS1, 2ms	Water suppression VAPOR (hermite 21.6 ms)
DW-spin echo with polychromatic pulse (PC-SE-LASER)	$\frac{\pi}{2}$: ahp, 2ms π: selective pulse on 0.9, 1.3, 2.0 and 3.5 ppm: 50 ms	t_d = 53.2 ms TE = 58.3 ms TR = 2 s (4 s for MM)	TE = 25 ms Adiabatic pulses: HS1, 2ms	No water suppression

B.

Sequences	Pulses	Diffusion Time(t_d) / Echo Time (TE)/ Repetition Time (TR)	Acquisition LASER parameters	Other sequence parameters
DW-non-selective stimulated echo sequence (STE-LASER)	$\frac{\pi}{2}$: Broad pulse: 0.1 ms.	t_d = 42.3 ms TE = 8.4 ms TR = 2 s (4 s for MM)	TE = 25 ms Adiabatic pulses: HS1, 2ms	Water suppression VAPOR (hermite 21.6 ms)
DW-spin echo with single-band pulse (SB-SE-LASER)	$\frac{\pi}{2}$: ahp, 2ms π: selective pulse on the 0.1-4.0 ppm: 5 ms	t_d = 42.3 ms TE = 47.4 ms TR = 2 s (4 s for MM)	TE = 25 ms Adiabatic pulses: HS1, 2ms	No water suppression

C.

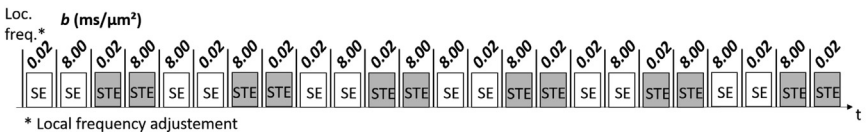

Fig. 2. Sequence parameters in both experiments. A) Comparisons between STE-LASER and PC-SE-LASER. B) Comparisons between STE-LASER and SB-SE-LASER. C) Diagram showing how acquisition blocks (32 repetitions each) are interleaved.

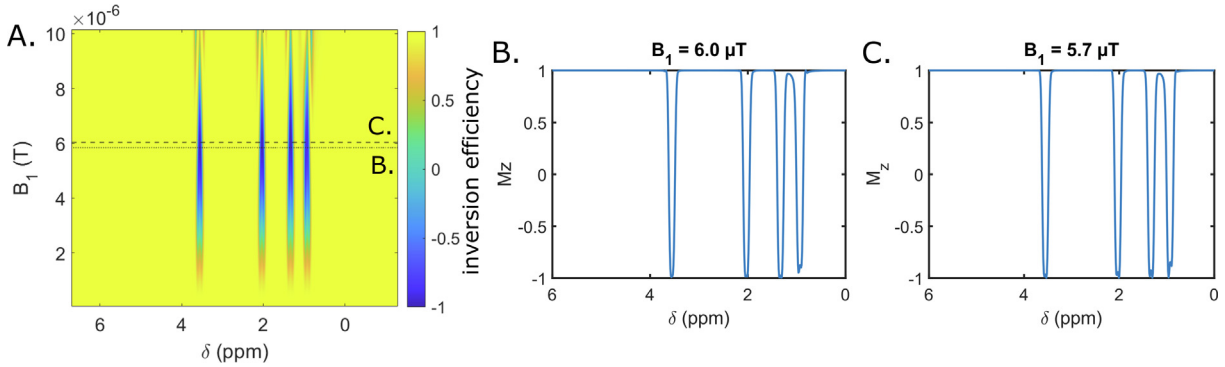

Fig. 3. A) Polychromatic pulse performance evaluated with Bloch simulations as a function of chemical shift δ and B_1; Frequency profiles for B) B_1 = 6.0 µT and for C) B_1 = 5.7 µT.

(not shown in Fig. 1A). In contrast, for both SE-LASER sequences, no water suppression was required, as water signal is not refocused in the SE block. Finally, MM spectrum (256 averages) was acquired for all sequences using a double inversion recovery module (TI_1 = 2200 ms and TI_2 = 770 ms), at b = 10 ms/µm^2 for further metabolite suppression.

Note that the minimal diffusion time t_d which can be achieved with the STE-LASER sequence is 42.3 ms, due to the water suppression pulse during mixing time. Hence, for the SB-SE-LASER *versus* STE-LASER comparison, t_d = 42.3 ms was used for both sequences (Fig. 2B). However, in the PC-SE-LASER, the 50-ms polychromatic pulse imposes a minimal t_d of 53.2 ms, which was used for both sequences for the PC-SE-LASER *versus* STE-LASER comparison (Fig. 2A).

2.5. Spectra analysis

Individual scans were phase- and frequency-corrected by home-made routines, before summation [15]. Then, spectra were

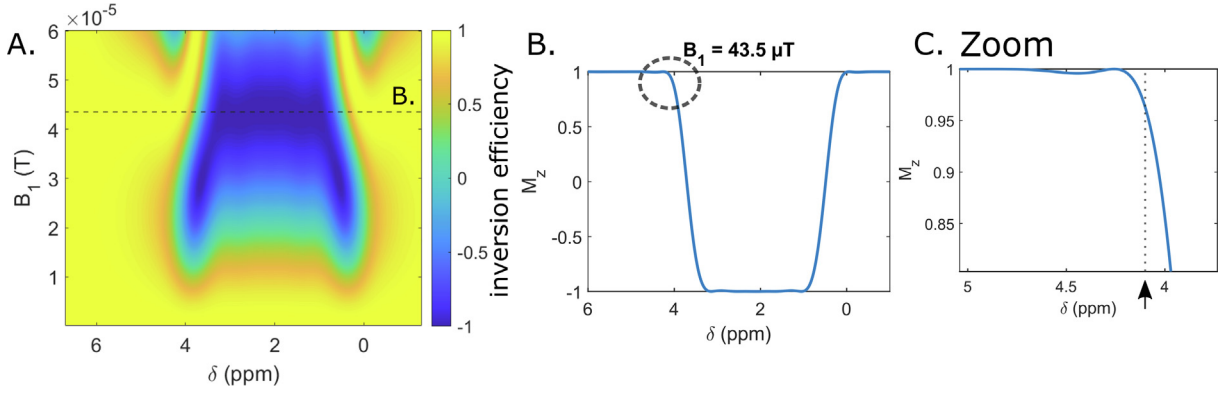

Fig. 4. A) Single-band pulse performance evaluated with Bloch simulations as a function of chemical shift δ and B_1. B) Frequency profile for the optimal B_1 = 43.5 µT. C) Zoom on the profile's "foot", showing very moderate (but not null) effect at 4.1 ppm (arrow), where lactate CH resonates.

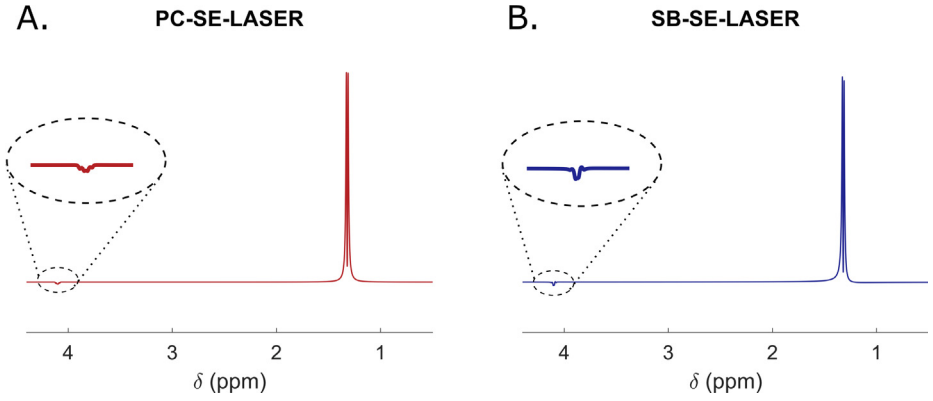

Fig. 5. Simulated lactate spectrum obtained with SE-LASER sequence using A) the polychromatic pulse or B) the single-band pulse. Total TE is 83.3 ms in the PC case (58.3 ms for the SE part and 25 ms for the LASER part), and 72.4 ms for the SB case (47.4 ms for the SE part and 25 ms for the LASER part). J-modulation is greatly suppressed on the 1.3 ppm resonance in both cases, but slightly less for the SB pulse, which may possibly be ascribed to the slightly larger residual signal refocused at 4.1 ppm. Spectra are shown with the same vertical scaling. A 15-Hz line broadening was applied to mimick in vivo conditions.

quantified using LCModel [16], with basis-sets including simulated metabolite spectra and experimental MM spectra.

3. Results

3.1. Simulations

The simulated profile of the polychromatic pulse barely changes when B_1 varies close to the optimal value of ~6.0 μT (Fig. 3). The bandwidth of each band is 0.14 ppm ± 0.01 ppm on average on the four bands, i.e. 70 Hz compared to the expected 78 Hz, i.e. a relative deviation of ~10%, related to the spectral resolution of the simulation.

Bloch simulations for the single-band pulse (Fig. 4) shows that the optimal B_1 is 43.5 μT. For this B_1, refocusing occurs on a 0.1–4.0 ppm band, as expected (Fig. 4B). Transition width is quite large (~0.9 ppm), so that the 4.1 ppm region (where the lactate CH group resonates) is not fully outside the transition band (Fig. 4C).

Lactate spectra simulated for the SE-LASER sequences using either the polychromatic or the single-band pulse are shown in Fig. 5, demonstrating the suppression of J-modulation. Due to the fact that the lactate peak at 4.1 ppm is slightly refocused (~7% of the signal at 4.1 ppm actually remains), suppression of J-modulation with the SB pulse is less perfect than with the PC pulse, but still largely efficient. Note that J-modulation during the LASER block is negligible, because that block behaves like a CPMG sequence with short echo spacing compared to J-modulation [17].

3.2. PC-SE-LASER vs. STE-LASER in vivo

In Fig. 6A-B, the selectivity of the polychromatic pulse on the 3 metabolites (Ins, tNAA = NAA + N-Acetylaspartylglutamate (NAAG), and Lac) and MM, as well as overall spectral quality, can be assessed at both *b*-values. The 1.3-ppm lactate peak is clearly more intense (by approximately a factor 2) with the PC-SE-LASER than with the STE-LASER.

tNAA peak is also more intense (approximately + 60% when comparing peak amplitude at 2.0 ppm) with the PC-SE-LASER than with the STE-LASER. The inositol peak at 3.5 ppm is fairly distorted, nevertheless its intensity is quite similar for both sequences. Finally, the MM signal at 0.9 ppm is slightly lower with the selective SE than with the STE, which is not surprising considering MM's short T_2.

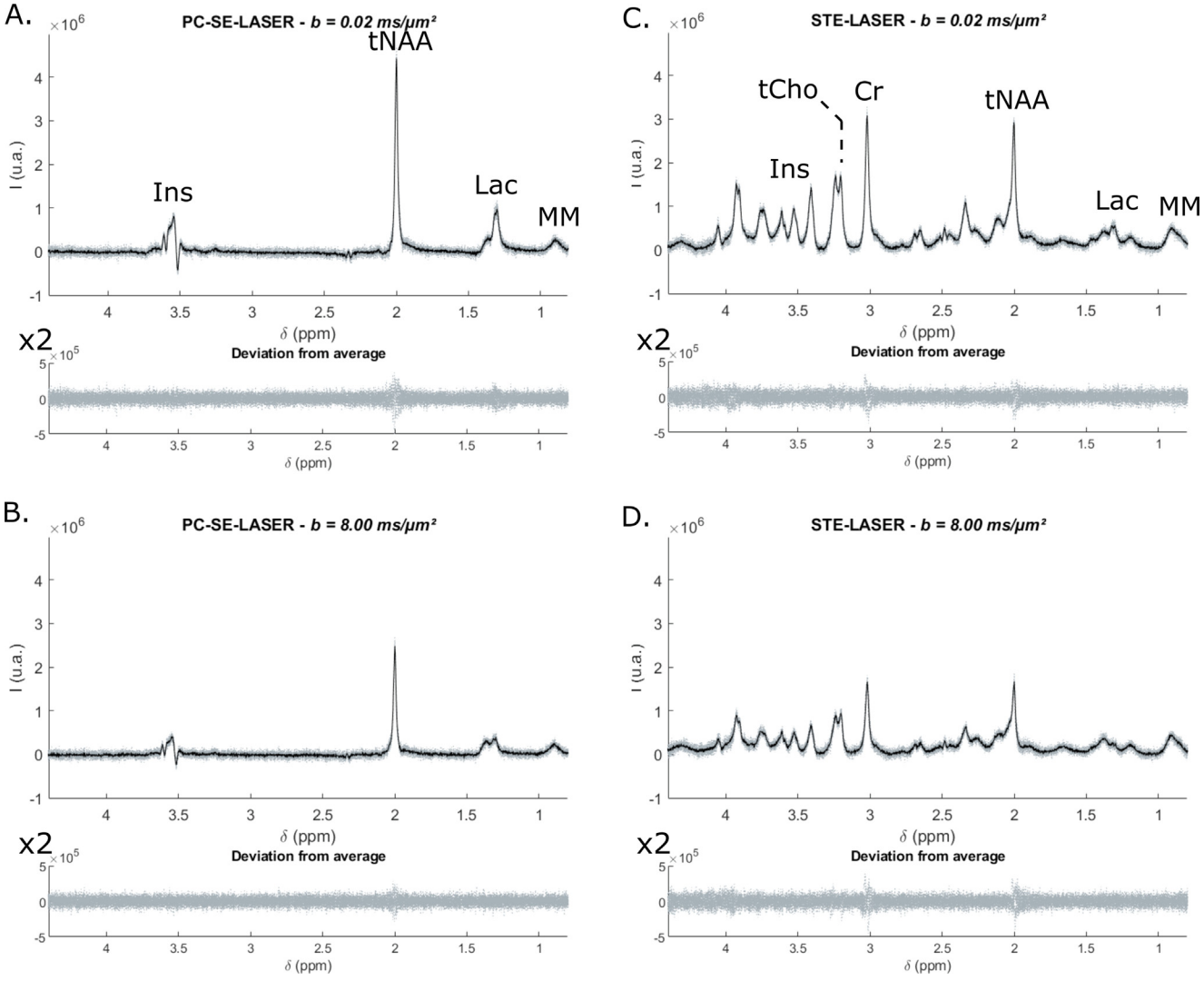

Fig. 6. *In vivo* acquisitions for A) the PC-SE-LASER at b = 0.02 ms/μm^2; B) the PC-SE-LASER at b = 8 ms/μm^2; C) the STE-LASER at b = 0.02 ms/μm^2; and D) the STE-LASER at b = 8 ms/μm^2. In order to illustrate spectral stability throughout the experiment, in each panel, the eight spectra (32 averages each) are plotted in gray, while the average spectrum is plotted in black. Deviation of each of the eight spectrum from mean spectrum is plotted in the bottom graph.

LCModel analysis is of reasonable quality (Fig. 7), although some residual signal around Ins peaks seems not accounted for when using the PC-SE-LASER. This could be due to a poor estimation of the Ins signal with the PC-SE-LASER, due to imperfect Ins spectrum in LCModel's basis-set. Nevertheless, Lactate signal appears to be doubled with PC-SE-LASER. Quantification reliability as estimated by LCModel is given by Cramer-Rào lower bounds (CRLBs), as reported in Fig. 8: lactate quantification appears more reliable when using PC-SE-LASER, especially at high *b* where CRLB is ~4% with the PC-SE-LASER *versus* ~10% for the STE-LASER; for tNAA there is only a moderate benefit, at high *b*; and for Ins and MM quantification seems slightly degraded but CRLBs remain within acceptable limits (<5%).

Assessing the benefits of using PC-SE-LASER for diffusion measurements might also be done by comparing the coefficient of variation (COV) of signal attenuation S(b = 8 ms/μm^2)/S(b = 0.02 ms/μm^2), calculated over the eight series (Fig. 9B). It appears that COV of signal attenuation is indeed significantly lower for lactate with the PC-SE-LASER (COV ~2% vs ~6% for the STE-LASER, with a 95% confidence level as assessed by one-way Fisher test). No statistically significant difference is found for other metabolites. Moreover, the mean value of the attenuation remains almost the same with both methods, for all metabolites (Fig. 9A).

3.3. SB-SE-LASER vs. STE-LASER in vivo

With the single-band pulse, all metabolites in the 0.1–4.0 ppm range are visible (Fig. 10). Lactate signal is again approximately twice larger than with STE-LASER. Total NAA (tNAA = NAA + NAA G), total creatine (tCr = Creatine Cr + Phosphocreatine PCr) and choline compounds (tCho = Choline + Phosphocholine PCho + Glycerophosphorylcholine GPC) are also clearly increased (approximately 80%). In contrast, Ins overall amplitude seems rather unchanged, which might be due to the combined effect of J-coupling, T_2 relaxation and the fact that Ins falls on the edge of the SB pulse frequency profile all counterbalancing the potential benefit of doubling observable magnetization thanks to SE compared to STE. MM signal at 0.9 ppm is much weaker with SB-SE-LASER than with STE-LASER.

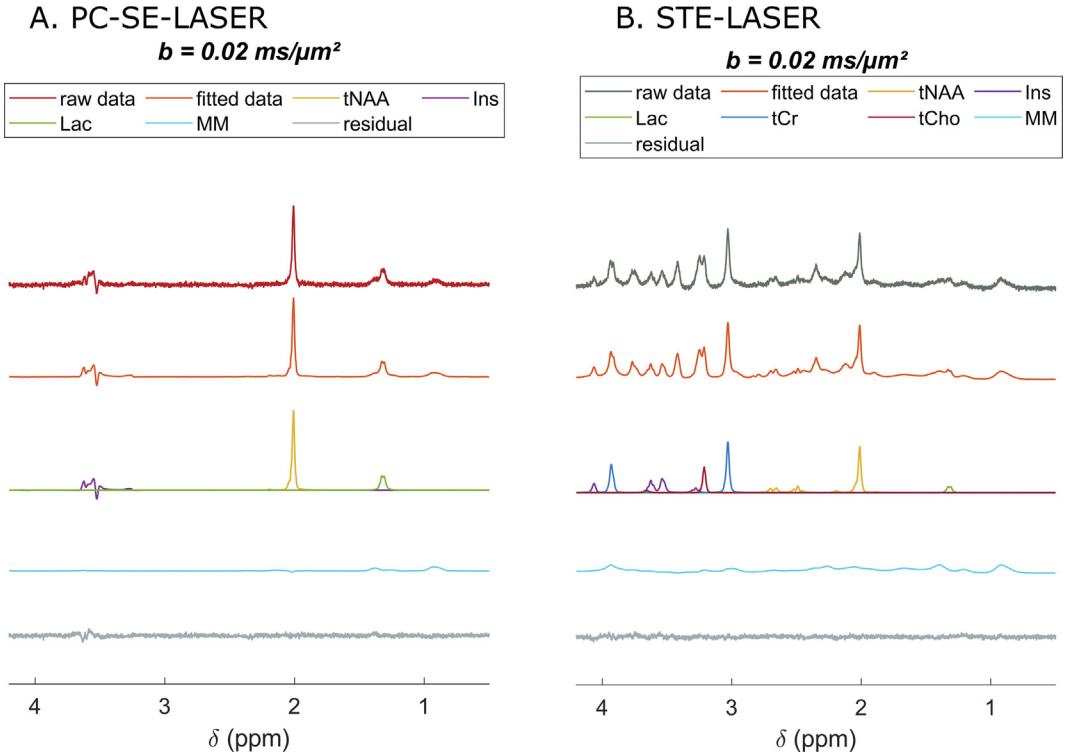

Fig. 7. Example of LCModel analysis for acquisitions performed at b = 0.02 ms/μm^2 with A) PC-SE-LASER and B) STE-LASER. Spectra are displayed with the same vertical scale.

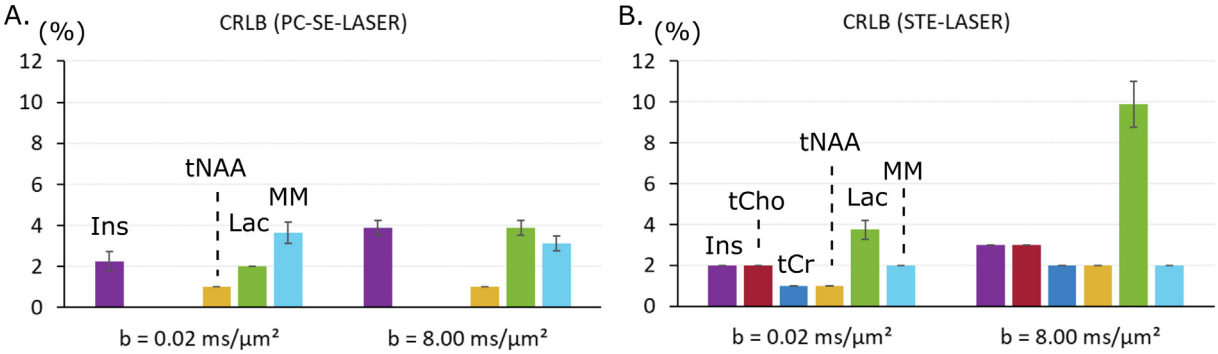

Fig. 8. LCModel's Cramer-Rào lower bounds (mean and s.d. computed over the eight series) for metabolites measured with A) PC-SE-LASER and B) STE-LASER.

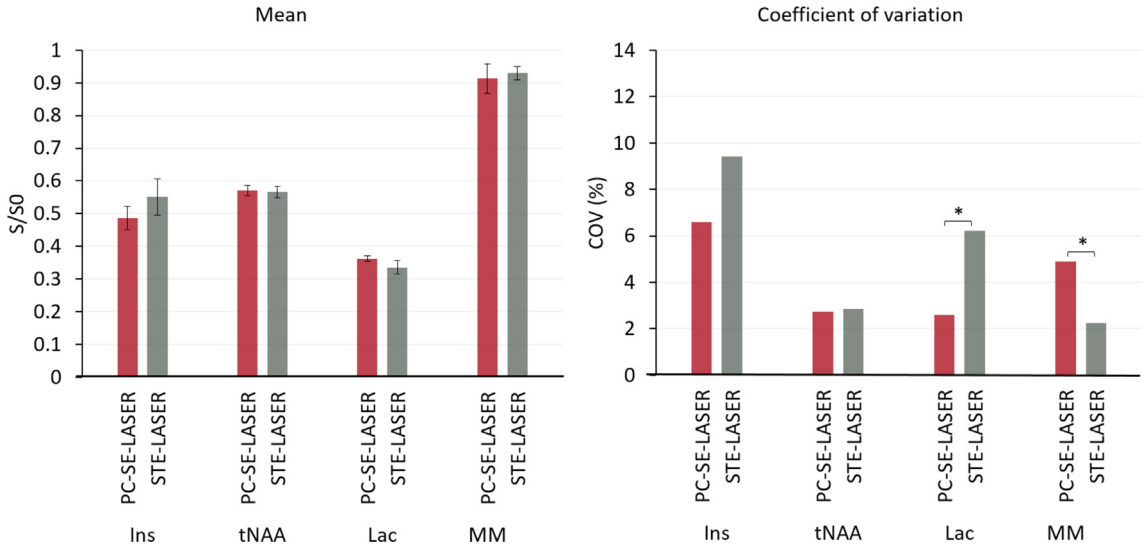

Fig. 9. A) Mean and standard deviation of signal attenuation $S/S_0 = S(b = 8\ ms/\mu m^2)/S(b = 0.02\ ms/\mu m^2)$ and B) coefficient of variation (COV) of signal attenuation on the eight series of acquisition, with PC-SE-LASER (in red) and STE-LASER (in gray). For lactate, COV is indeed lower (with a 95% significance, one-way Fisher test) with PC-SE-LASER than with STE-LASER. (For interpretation of the references to colour in this figure legend, the reader is referred to the web version of this article.)

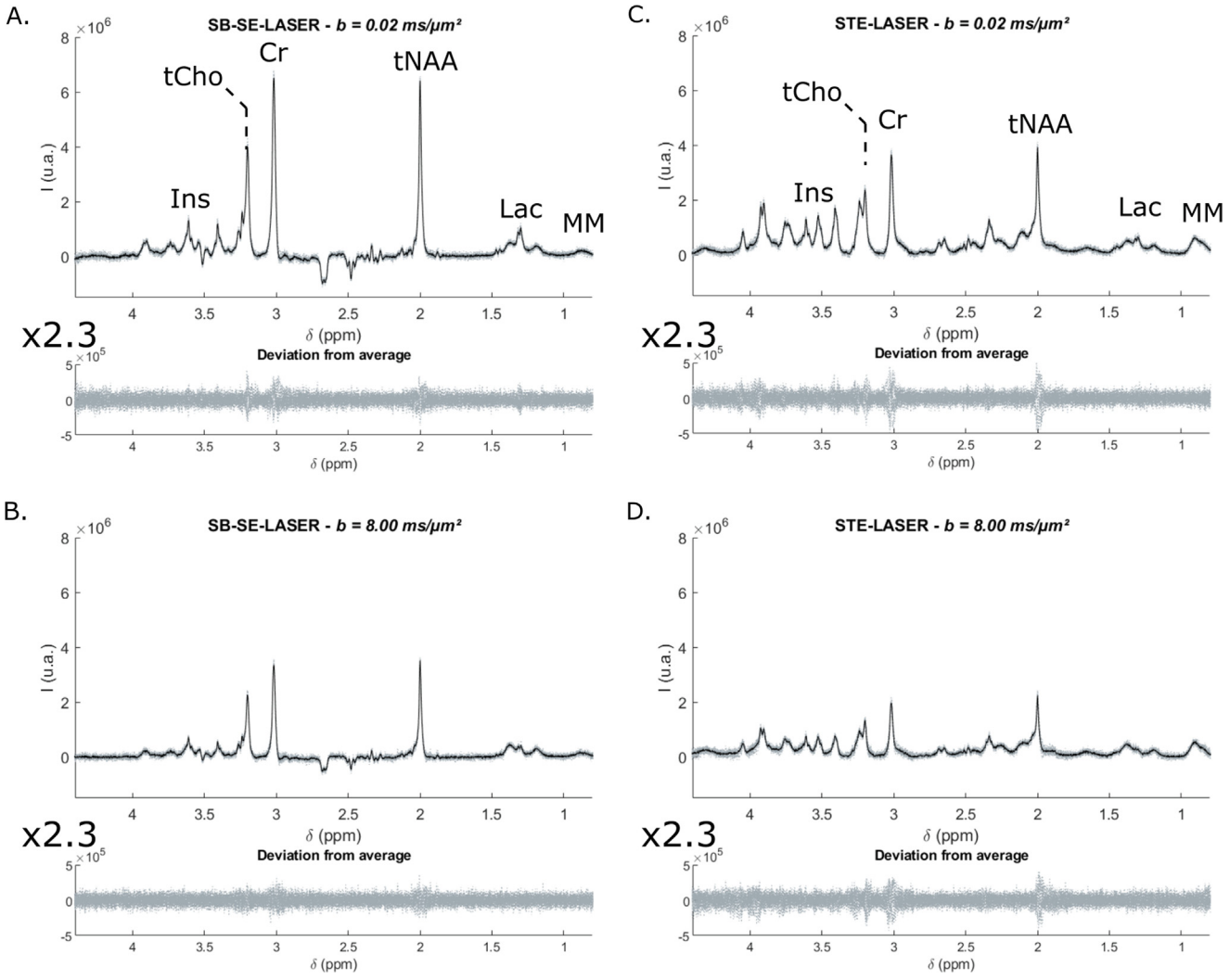

Fig. 10. *In vivo* acquisitions for A) the SB-SE-LASER at $b = 0.02\ ms/\mu m^2$; B) the SB-SE-LASER at $b = 8\ ms/\mu m^2$; C) the STE-LASER at $b = 0.02\ ms/\mu m^2$; and D) the STE-LASER at $b = 8\ ms/\mu m^2$. In order to illustrate spectral stability throughout the experiment, in each panel, the eight spectra (32 averages each) are plotted in gray, while the average spectrum is plotted in black. Deviation of each of the eight spectrum from mean spectrum is plotted in the bottom graph.

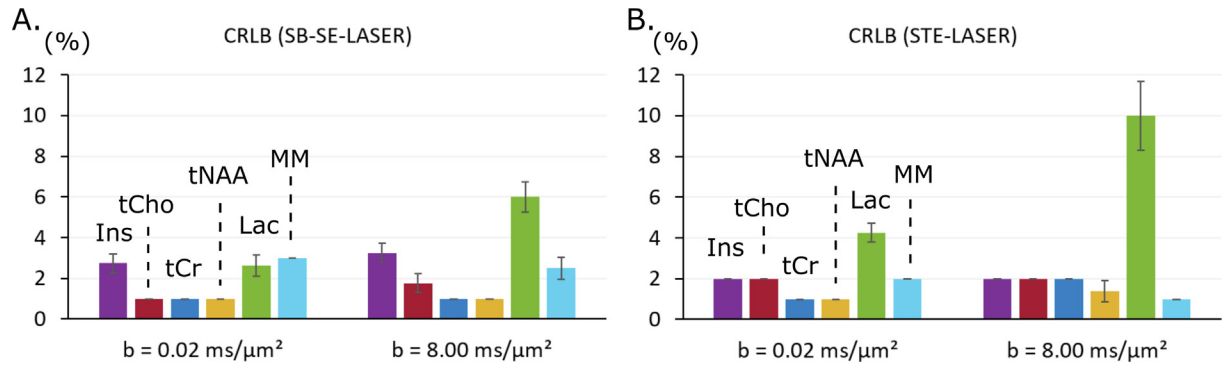

Fig. 11. LCModel's Cramer-Rào lower bounds (mean and s.d. computed over the eight series) for metabolites measured with A) SB-SE-LASER and B) STE-LASER.

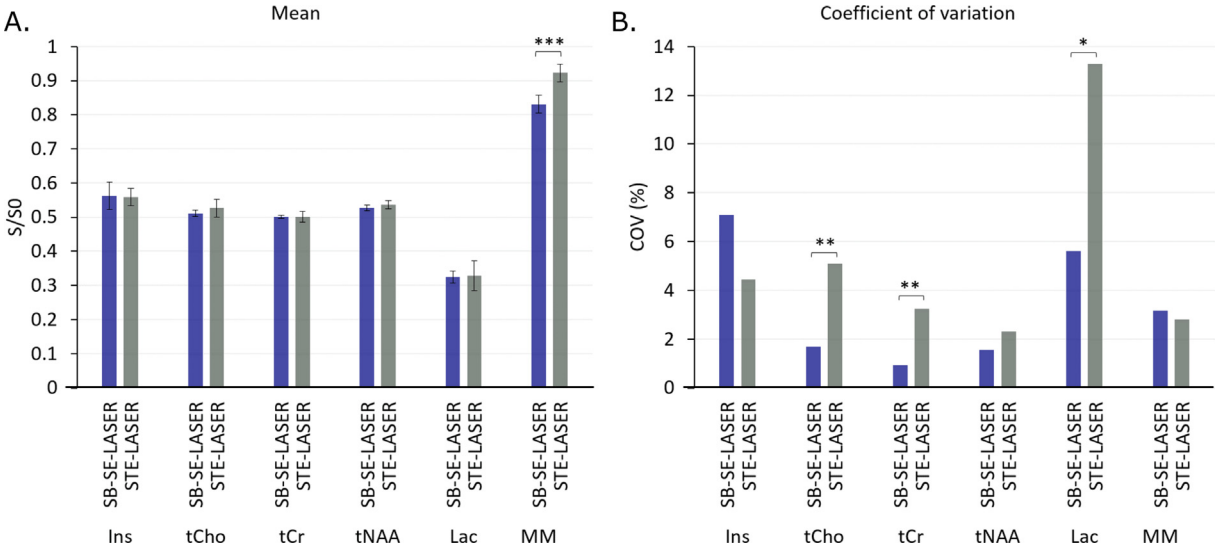

Fig. 12. A) Mean and standard deviation of signal attenuation $S/S_0 = S(b = 8\ ms/\mu m^2)/S(b = 0.02\ ms/\mu m^2)$ and B) coefficient of variation (COV) of signal attenuation on the eight series of acquisition, with SB-SE-LASER (in blue) and the STE-LASER (in gray). COV is lower with SB-SE-LASER for lactate (95% significance, one-way Fisher test) and for tCho and tCr (99% significance). (For interpretation of the references to colour in this figure legend, the reader is referred to the web version of this article.)

When looking at LCModel's CRLBs (Fig. 11), estimated precisions on metabolite signal is similar with both sequences for tNAA, tCr and tCho, at low *b*-value. At higher *b*-value, CRLBs are lower with the SB-SE-LASER for tNAA and tCr, but identical for tCho. Ins and MM estimations seems to be slightly less precise with the SB-SE-LASER. Here again, CLRB on lactate appears smaller with the SB-SE-LASER (~3% at $b = 0.02\ ms/\mu m^2$ and 6% at $b = 8\ ms/\mu m^2$, *versus* ~4% at $b = 0.02\ ms/\mu m^2$ and 10% at $b = 8\ ms/\mu m^2$ with STE-LASER).

Finally, COV of signal attenuation is significantly lower with SB-SE-LASER for tCho, tCr and Lac (Fig. 12B), but tends to be larger (although not significantly) for Ins and MM, which is overall in line with peak heights and CRLB as reported above. No significant variation of mean attenuation is observed (except for MM). This confirms higher precision of lactate measurement with SB-SE-LASER.

4. Discussion

4.1. Going from STE to SE: Expected signal gains for singlets

For a singlet such as the CH_3 group of NAA, going from STE to SE is expected to result in a maximal 2-fold signal gain. However, for a given diffusion time, signal gain will be lower than that because of relaxation. For the SE-LASER, we will make the approximation t_d =~ TE (the echo time in the SE block, without the LASER block), so that signal is given by $S_{SE} \sim S_0 \times \exp(-t_d/T_2)$; for the STE-LASER we will use the approximation t_d = TM, and we will neglect T_2 relaxation during the short TE of the STE block (8.4 ms), i.e. $S_{STE} = S_0/2 \times \exp(-t_d/T_1)$. T_2 relaxation during the LASER module is not considered, as it is the same in both sequences. Considering $T_2 \sim 280$ ms and $T_1 \sim 1710$ ms [10] for NAA at 11.7 T, we hence expect between 70 and 80% signal gain for t_d as used in this study, which is actually in rather good agreement with the 60% and 75% signal gains observed for tNAA at both t_d used in this study. The slightly lower gain as compared to theory might be due to imperfect refocusing in the SE block, due to B_1 inhomogeneities.

Using the simplified expressions for S_{SE} and S_{STE} as given above, one can also predict that SE-LASER is expected to outperform STE-LASER for singlet detection as long as t_d is shorter than 200–250 ms. For longer t_d, STE-LASER should be preferred even for peaks unaffected by J-coupling.

4.2. Simply going from STE to SE does not improve lactate signal, but J-modulation suppression does

When refocusing in the SE block is achieved with a spectrally-selective pulse excluding lactate CH group at 4.1 ppm, increased lactate signal at 1.3 ppm is obtained as compared to STE-LASER sequence. Importantly, this signal increase is not simply due to larger magnetization available in SE as compared to STE, as would be the case for a singlet (see section 4.1 above). This can be demonstrated by replacing the spectrally-selective refocusing pulse by a

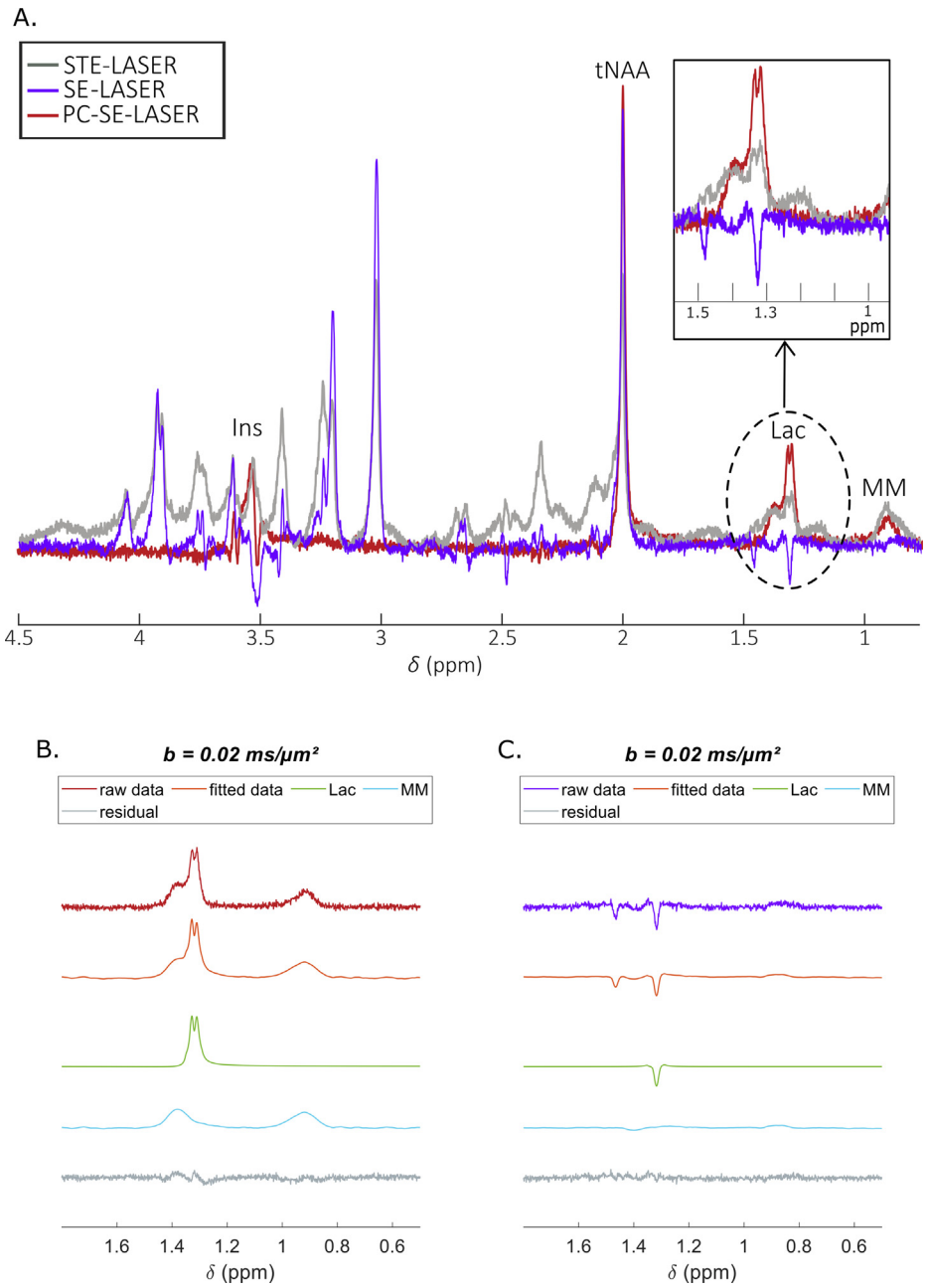

Fig. 13. Illustration of the benefit of using a spectrally-selective refocusing pulse. A) A spectrum acquired with a STE-LASER sequence (gray) is overlaid with a spectrum acquired with a PC-SE-LASER sequence (red). Increased lactate signal at 1.3 ppm can be clearly appreciated, despite the much increased TE in the PC-SE-LASER (83.3 ms vs 33.4 ms for the STE-LASER). Such signal increase cannot be simply attributed to larger magnetization available with SE, as can be easily assessed by replacing the PC pulse by a broad pulse in the SE-LASER sequence (purple). B)-C) On spectral decompositions extracted from LCModel analysis, lactate signal (green) is clearly more intense with the PC-SE-LASER (B) than with the SE-LASER (C), and the MM signal (light blue) is lower with the SE-LASER (the scales are identical on B and C). (For interpretation of the references to colour in this figure legend, the reader is referred to the web version of this article.)

broad pulse in the SE block, e.g. as illustrated in Fig. 13A for PC pulse *versus* broad pulse. LCModel decompositions provide a closer look at the actual gain for lactate, once MM contribution has been removed (Fig. 13B and C), confirming a much larger lactate signal in the PC case. Intriguingly, in this comparison MM signal at 0.9 and 1.3 ppm appears more prominent with the polychromatic than with the broad pulse. This might be due to some J-coupling between these MM peaks and some other MM resonances, which would be at least partially cancelled with the PC-SE-LASER.

In the end, we estimate that lactate signal is increased by a factor ~2 for the PC-SE-LASER *versus* STE-LASER, and ~1.9 for the SB-SE-LASER *versus* STE-LASER, as estimated by measuring the peak height after removing MM signal (while peak height can be affected by linewidth, here the linewidth does not change, due to the interlaced acquisitions). The small difference in gain observed between the two pulses is certainly due to the fact that SB pulse is not as selective as the PC and refocuses slightly more the 4.1-ppm resonance.

4.3. Some caveats of PC- and SB-SE-LASER

Because of the very narrow bandwidth of the elementary pulses, PC-SE-LASER might possibly be less robust than SB-SE-LASER to small frequency fluctuations or shim degradations during the experiment. We think this is likely to explain the fact that, despite larger signal, COV on NAA signal attenuation is almost

identical between PC-SE-LASER acquisition and STE-LASER acquisition, despite larger signal with the PC-SE-LASER, whereas COV on NAA is much lower for SB-SE-LASER. Another advantage of the SB-SE-LASER is that it potentially enables measurements at shorter diffusion time than with PC-SE-LASER. However, SB-SE-LASER might be slightly less efficient than PC-SB-LASER to suppress the effect of J-coupling on the CH_3 lactate resonance, due to slightly larger residual refocusing of the coupling partner at 4.1 ppm. Myo-inositol appears to be quite distorted when using SE-LASER with selective refocusing. This is certainly due to the fact that resonances of Ins do not all experience perfect refocusing. Indeed, the elementary bandwidth of the PC pulse is too low to perform perfect refocusing across the whole chemical shift range of Ins resonances (~3.25–4.05 ppm). In the case of the SB pulse, the resonances lie right on the transition band. Hence, with PC or SB, Ins lineshape will not only be complex, but also very sensitive to frequency shift and B_0 inhomogeneity. Quantification of myo-inositol therefore remains challenging on such spectra, and might be improved in the future.

In general, the weaknesses associated with SB or PC pulses as mentioned above are expected to be mitigated when going at fields higher than 11.7 T, due to increased frequency dispersion between the different resonances of interest, allowing shorter RF pulses and larger (in Hz) transition bands.

5. Conclusion

By suppressing J-modulation, SE-LASER with a spectrally-selective refocusing pulse appears to be efficient to measure lactate attenuation at high *b*-values, while in the meantime retaining signal for other metabolites of interest (NAA and Ins). The two selective pulses investigated here, polychromatic and single-band, are overall similarly efficient, however they have specific limits and advantages. On one hand, the polychromatic pulse is slightly more selective, and hence provides slightly more signal on Lac and Ins, but is also more sensitive to frequency drifts or shim degradation. This pulse can thus be useful for the specific study of the lactate compartmentation in a small voxel where SNR is critically limited but B_0 very stable. On the other hand, the single-band pulse is more robust when B_0 is less stable, allows measuring more metabolites, and due to its shorter duration may allow reaching shorter TE and diffusion time if needed. Overall, going at field strengths even higher than 11.7 T might increase the benefit of using spectrally-selective pulses, as larger frequency dispersion between resonances impose less constraints on pulse profile and duration.

Funding

This project has received funding from the European Research Council (ERC) under the European Union's Horizon 2020 research and innovation programmes (grant agreement No 818266).

Declaration of Competing Interest

The authors declare that they have no known competing financial interests or personal relationships that could have appeared to influence the work reported in this paper.

Acknowledgement

None.

References

[1] J. Pfeuffer, I. Tkác, R. Gruetter, Extracellular-intracellular distribution of glucose and lactate in the rat brain assessed noninvasively by diffusion-weighted 1H nuclear magnetic resonance spectroscopy in vivo, J. Cereb. Blood Flow Metab. Off. J. Int. Soc. Cereb. Blood Flow Metab. 20 (2000) 736–746, https://doi.org/10.1097/00004647-200004000-00011.

[2] M. Palombo, C. Ligneul, J. Valette, Modeling diffusion of intracellular metabolites in the mouse brain up to very high diffusion-weighting: Diffusion in long fibers (almost) accounts for non-monoexponential attenuation, Magn. Reson. Med. 77 (2017) 343–350, https://doi.org/10.1002/mrm.26548.

[3] M. Palombo, C. Ligneul, C. Najac, J. Le Douce, J. Flament, C. Escartin, P. Hantraye, E. Brouillet, G. Bonvento, J. Valette, New paradigm to assess brain cell morphology by diffusion-weighted MR spectroscopy in vivo, Proc. Natl. Acad. Sci. U. S. A. 113 (2016) 6671–6676, https://doi.org/10.1073/pnas.1504327113.

[4] N. Shemesh, J.T. Rosenberg, J.-N. Dumez, S.C. Grant, L. Frydman, Distinguishing neuronal from astrocytic subcellular microstructures using in vivo Double Diffusion Encoded 1H MRS at 21.1 T, PLOS ONE. 12 (2017), https://doi.org/10.1371/journal.pone.0185232 e0185232.

[5] C. Ligneul, M. Palombo, E. Hernández-Garzón, M.-A. Carrillo-de Sauvage, J. Flament, P. Hantraye, E. Brouillet, G. Bonvento, C. Escartin, J. Valette, Diffusion-weighted magnetic resonance spectroscopy enables cell-specific monitoring of astrocyte reactivity in vivo, NeuroImage. 191 (2019) 457–469, https://doi.org/10.1016/j.neuroimage.2019.02.046.

[6] L. Pellerin, P.J. Magistretti, Glutamate uptake into astrocytes stimulates aerobic glycolysis: a mechanism coupling neuronal activity to glucose utilization, Proc. Natl. Acad. Sci. 91 (1994) 10625–10629, https://doi.org/10.1073/pnas.91.22.10625.

[7] P. Mächler, M.T. Wyss, M. Elsayed, J. Stobart, R. Gutierrez, A. von Faber-Castell, V. Kaelin, M. Zuend, A. San Martín, I. Romero-Gómez, F. Baeza-Lehnert, S. Lengacher, B.L. Schneider, P. Aebischer, P.J. Magistretti, L.F. Barros, B. Weber, Vivo Evidence for a Lactate Gradient from Astrocytes to Neurons, Cell Metab. 23 (2016) 94–102, https://doi.org/10.1016/j.cmet.2015.10.010.

[8] F. Yamasaki, J. Takaba, M. Ohtaki, N. Abe, Y. Kajiwara, T. Saito, H. Yoshioka, S. Hama, T. Akimitsu, K. Sugiyama, K. Arita, K. Kurisu, Detection and differentiation of lactate and lipids by single-voxel proton MR spectroscopy, Neurosurg. Rev. 28 (2005) 267–277, https://doi.org/10.1007/s10143-005-0398-1.

[9] M. Dacko, T. Lange, Flexible MEGA editing scheme with asymmetric adiabatic pulses applied for measurement of lactate in human brain, Magn. Reson. Med. 85 (2021) 1160–1174, https://doi.org/10.1002/mrm.28500.

[10] R.A. de Graaf, P.B. Brown, S. McIntyre, T.W. Nixon, K.L. Behar, D.L. Rothman, High magnetic field water and metabolite proton T1 and T2 relaxation in rat brain in vivo, Magn. Reson. Med. 56 (2006) 386–394, https://doi.org/10.1002/mrm.20946.

[11] C. Ligneul, M. Palombo, J. Valette, Metabolite diffusion up to very high b in the mouse brain in vivo: Revisiting the potential correlation between relaxation and diffusion properties, Magn. Reson. Med. 77 (2017) 1390–1398, https://doi.org/10.1002/mrm.26217.

[12] N. Shemesh, J.T. Rosenberg, J.-N. Dumez, J.A. Muniz, S.C. Grant, L. Frydman, Metabolic properties in stroked rats revealed by relaxation-enhanced magnetic resonance spectroscopy at ultrahigh fields, Nat. Commun. 5 (2014) 4958, https://doi.org/10.1038/ncomms5958.

[13] J. Pauly, P. Le Roux, D. Nishimura, A. Macovski, Parameter relations for the Shinnar-Le Roux selective excitation pulse design algorithm (NMR imaging), IEEE Trans. Med. Imaging. 10 (1991) 53–65, https://doi.org/10.1109/42.75611.

[14] V. Govindaraju, K. Young, A.A. Maudsley, Proton NMR chemical shifts and coupling constants for brain metabolites, NMR Biomed. 13 (2000) 129–153, https://doi.org/10.1002/1099-1492(200005)13:3<129::AID-NBM619>3.0.CO;2-V.

[15] S. Posse, C.A. Cuenod, D. Le Bihan, Human brain: proton diffusion MR spectroscopy, Radiology. 188 (1993) 719–725, https://doi.org/10.1148/radiology.188.3.8351339.

[16] S.W. Provencher, Automatic quantitation of localized in vivo 1H spectra with LCModel, NMR Biomed. 14 (2001) 260–264, https://doi.org/10.1002/nbm.698.

[17] L.A. Stables, R.P. Kennan, A.W. Anderson, J.C. Gore, Density Matrix Simulations of the Effects of J Coupling in Spin Echo and Fast Spin Echo Imaging, J. Magn. Reson. 140 (1999) 305–314, https://doi.org/10.1006/jmre.1998.1655.